IAC-21.C1.4.6

LUNAR FROZEN ORBITS FOR SMALL SATELLITE COMMUNICATION/NAVIGATION CONSTELLATIONS

Maksim Shirobokov
Keldysh Institute of Applied Mathematics, RAS, Russian Federation, shirobokov@keldysh.ru

Sergey Trofimov
Keldysh Institute of Applied Mathematics, RAS, Russian Federation, trofimov@keldysh.ru
Mikhail Ovchinnikov
Keldysh Institute of Applied Mathematics, RAS, Russian Federation, ovchinni@keldysh.ru

Recent strategies of lunar exploration developed by the world's leading space agencies stimulate building the communication and navigation infrastructure in the circumlunar space. However, contrary to existing Earth-orbiting constellations, a lunar distributed satellite system requires a much higher deployment and maintenance cost. Moreover, the dynamical environment in the vicinity of the Moon is known to be much more complex, which prevents using most of the developed constellation theories based on Keplerian orbits or J_2-perturbed orbits. The orbital stability is of particular concern for small satellite constellations. Such constellations must be placed in low to medium lunar orbits due to antenna size/power limitations. On the one hand, this ensures low signal latency and eases the establishment of inter-satellite links. On the other hand, to avoid prohibitively high station-keeping costs, one needs to find a solution to the far from trivial problem of how to select proper frozen orbits (orbits with the nearly constant eccentricity and argument of periapsis values) for tens or even hundreds of satellites in the constellation. In this paper, we investigate low and medium frozen orbits of different altitude and inclination from the viewpoint of stability, Moon's surface coverage, and revisit times for specified lunar sites. The approach to choosing an accurate enough dynamical model is described. The numerical technique based on the Bayesian optimization is put forward for the design of frozen and quasi-frozen (slowly drifting) orbits. The dependency of mean revisit time on the number of satellites in (quasi-)frozen orbits and orbital planes is investigated. The minimum number of small satellites required for the 1-fold and 4-fold global coverage is estimated for a constellation in low near-polar lunar orbits. The augmentation with several satellites in a medium polar orbit is also studied to enhance visibility. Of special focus is the coverage properties for the craters of Boguslawsky and Manzinus, the primary and backup landing sites of the Russian Luna 25 probe scheduled for launch in May 2022.

I. INTRODUCTION

Satellite constellations have been serving for the purposes of communication and navigation for many years. Since the 1960s, the overwhelming majority of studies on the constellation design and optimization have been devoted to the Earth coverage problem. While communication applications nominally require a 1-fold coverage, positioning on the Earth's surface is provided with at least 4 satellites visible at any moment of time. To ensure the global coverage, a completely symmetrical orbital configuration is usually considered, with several orbital planes equally distributed around the globe and containing equal number of satellites. Such a regular configuration was first studied in the works of Walker [1] and Mozhaev [2, 3]. The latter researcher called it a kinematically regular network, which is a special case of symmetrical configurations Mozhaev studied using the group theory methods. However, the terminology of Walker constellation or Walker–Mozhaev constellation is now used much more frequently. The alternative approach to the constellation design is based on the street of coverage concept. It appeared even earlier and was exploited in designing constellations of zonal as well as global coverage [4–6]. The comparative analyses of different constellation design techniques have been publishing throughout the years [7–9].

Significant efforts have been put to the constellation design optimization. The theoretical minimum bound of $2N + 3$ satellites for the N-fold continuous coverage found by Ballard [10] for circular orbit constellations was later refined to $2N + 2$ by Draim [11–13] who considered the more general elliptical orbit case. For constellations with a large number of satellites, the search space is high-dimensional and the researchers usually resort to numerical global

optimization techniques, such as the genetic algorithms [8, 14–16]. This kind of methods can also be applied to discontinuous coverage problems, including the regional coverage problem [17], though for homogeneous constellations (with the same altitude and inclination for all the satellites), a simpler geometric approach was developed [18–20] based on two-dimensional maps of visibility properties. The zonal/regional coverage analysis and optimization can be conveniently performed in the Earth-fixed frame because satellite ground tracks are always "shadowed" (approximated with any given accuracy) by some repeating ground tracks. Such a trivial idea gave rise to the route constellation concept [21–24]. The route theory is also applicable to non-homogeneous (compound) constellations when the orbits of different satellites can be of different altitude and inclination, but the nodal regression is synchronized [25].

Another fruitful methodology of constellation design exploiting the rotating frame is the flower constellation theory [26–28]. The resonant orbits in this frame look like a flower with several petals, which gives name to the theory. If the rotating frame is the Earth-fixed frame, the satellites in a flower constellation are distributed along a single or multiple closed ground tracks. The harmonic flower constellations—the flower constellations possessing the highest degree of symmetry—are the counterpart of Walker–Mozhaev constellations. The strict mathematical formulation of the flower constellation theory—the 2D lattice theory of flower constellations—was developed by Avendaño et al. [29] who leveraged integer arithmetic and the lattice theory. The 2D lattice theory has then been extended to the 3D theory to include the case of elliptical orbits with synchronized apsidal rotation [30]. For non-homogeneous constellations, the 4D theory has been recently published [31]. A 4D lattice flower constellation consists of several 3D lattice flower constellations with different semimajor axis values. Flower constellations with a lower degree of symmetry are represented by the necklace, a lattice in which some positions are empty. These counterparts of Mozhaev's kinematically symmetrical constellations can be described using the necklace theory [32–34].

The current plans of lunar exploration developed by the leading space agencies implicitly or explicitly assume building the communication and navigation infrastructure in the near-lunar space. Contrary to Earth-orbiting constellations, lunar distributed satellite systems are much more expensive in deployment and maintenance. Furthermore, the orbital dynamics around the Moon are very complex, which prevents directly leveraging the above mentioned constellation theories based on Keplerian orbits or J_2-perturbed orbits. To minimize the number of satellites in a constellation, medium or high lunar orbits are of primary interest. In this case, the major perturbation is due to the Earth gravity. It makes near-polar orbits unstable. Therefore, Ely and Lieb [35,36] proposed to use mid-inclined (40 deg) orbits with the mean values of the eccentricity and the argument of periapsis both almost constant over a long time period. Six satellites in two orbital planes are proved to be sufficient for the global lunar coverage. An option of building a constellation in the vicinity of lunar libration points is thoroughly studied by many researchers as well. Halo orbits and distant retrograde orbits are mainly considered [37, 38]. The results of numerical comparative studies (see, e.g., [39, 40]) gave rise to various architectures of prospective lunar communication/navigation constellations [41–43].

The viable alternative to a group of large, expensive lunar satellites is a small satellite constellation. However, traditional constellation designs not exploiting natural dynamics demand too much fuel to counteract lunar perturbations: with a realistic monopropellant thruster, the constellation lifetime does not exceed several months [44]. So, lunar frozen orbits—natural orbits with the nearly constant eccentricity and argument of periapsis values—seem to be the only option for a small satellite constellation. It is especially true if, due to antenna size/power limitations, a constellation has to be placed in low orbits subject to strong perturbing influence of lunar gravity. There exist numerous analytical investigations on the frozen orbit design (the papers [45–48] describe just some of them), but the underlying perturbation theory becomes increasingly sophisticated as more realistic dynamical models are used.

In this paper, the numerical technique based on the Bayesian optimization is proposed for the design of frozen and quasi-frozen (slowly drifting) orbits. The approach to choosing an accurate enough dynamical model is described. We explore low to medium frozen orbits of different altitude and inclination from the aspects of stability, lunar surface coverage, and revisit times for specified sites. The dependency of mean revisit time on the number of satellites in (quasi-)frozen orbits and orbital planes is investigated. The minimum number of small satellites required for the 1-fold and 4-fold global coverage is estimated for a constellation in low near-polar lunar orbits. The augmentation with

several satellites in a medium polar orbit is also studied to enhance visibility. Of special attention is the coverage properties for Boguslawsky and Manzinus craters, the primary and backup landing sites of the Russian Luna 25 probe scheduled for launch in May 2022.

II. THE MODEL OF MOTION

In this section, we analyze perturbing forces that act on a Moon orbiting spacecraft and present a motion model for the following research.

First, a discrete set of points around the Moon is generated and at each point, we calculate the gravitational forces from the Moon, the Earth, and the Sun, as well as the solar radiation pressure (SRP) force. Specifically, we took 100 values of altitude in the interval from 50 km to 2 lunar radii (≈ 3500 km), 100 values of latitude from $-90°$ to $+90°$, and 100 values of longitude in the interval from $-180°$ to $+180°$. As a result, 9802 unique points have been generated. The lunar gravity force model includes the spherical harmonics perturbations up to degree and order 50. The SRP force was estimated for the area-to-mass ratio of 0.02 m^2/kg. At each altitude, among all the points the point delivering maximum to a perturbing acceleration relative to the local central gravitational acceleration is detected. The corresponding curves for each source of perturbation are depicted in Fig. 1. It shows that in a low to medium lunar orbit, the major perturbations come from the oblateness of the Moon and the Earth gravity. For orbits with an altitude lower than 2000 km, the perturbations due to the complex lunar gravity field dominate over other perturbations.

The contribution of each spherical harmonic into the magnitude of the harmonics perturbation depends on the altitude of the orbit. For each harmonic degree N, we calculated the maximum altitude at which the relative magnitude of the lunar gravity acceleration in the $N \times N$ model is less than some small ε; Fig. 2 shows the recovered dependencies (blue color) for $\varepsilon = 10^{-6}$ (Fig. 2a) and $\varepsilon = 10^{-7}$ (Fig. 2b). For practical applications, these dependencies are conveniently least square approximated (red color) over the class of power functions:

$$N = \left(\frac{25}{h[10^3 \text{ km}]}\right)^{0.8} \quad \text{for } \varepsilon = 10^{-6},$$

$$N = \left(\frac{40}{h[10^3 \text{ km}]}\right)^{0.8} \quad \text{for } \varepsilon = 10^{-7}.$$

In the denominator, the orbital altitude should be substituted in thousands km. The derived expressions can be used to estimate the maximum required degree in the spherical harmonics model of the lunar gravitational field in order to limit the computational burden while numerically propagating lunar orbits.

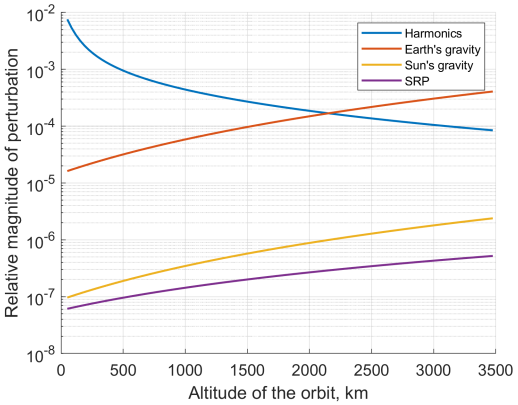

Fig. 1: Relative magnitude of perturbations as a function of the orbital altitude.

In this research, spacecraft trajectories are propagated numerically by the variable-order Adams method (the `ode113` routine in MATLAB) in the selenocentric celestial reference system (SCRS) whose axes are parallel to those of the International celestial reference system (ICRS). Equinoctial elements were used to speed up numerical integration of the equations of motion. The model of motion was restricted to the perturbations described above: the gravitational forces due to the Earth and the Sun, the SRP force, and the lunar spherical harmonics model in which the maximum expansion degree and order were chosen according to the above simple approximations. The positions of celestial bodies have been taken from JPL's DE430 ephemeris model.

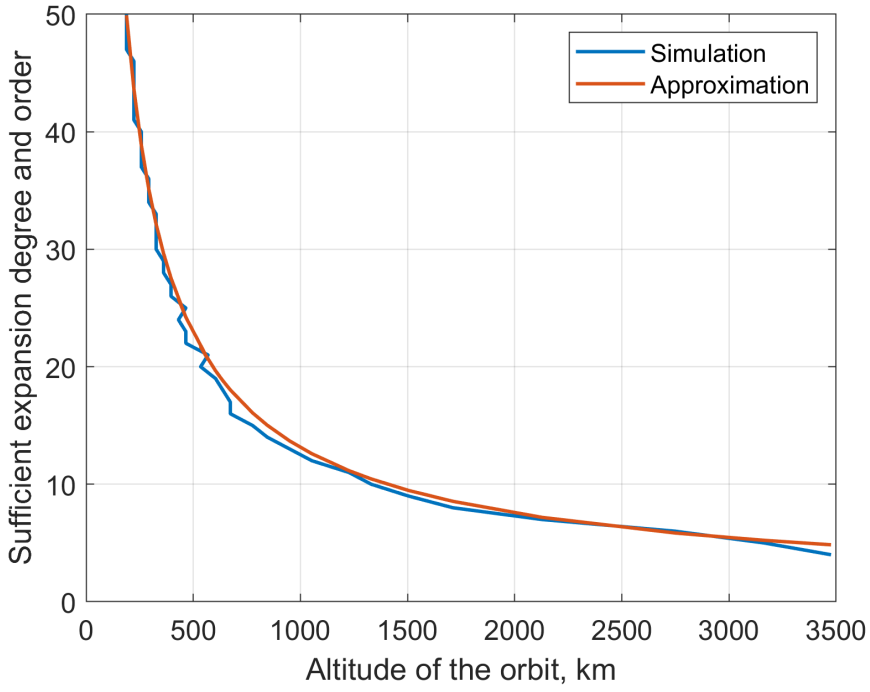

(a) $\varepsilon = 10^{-6}$

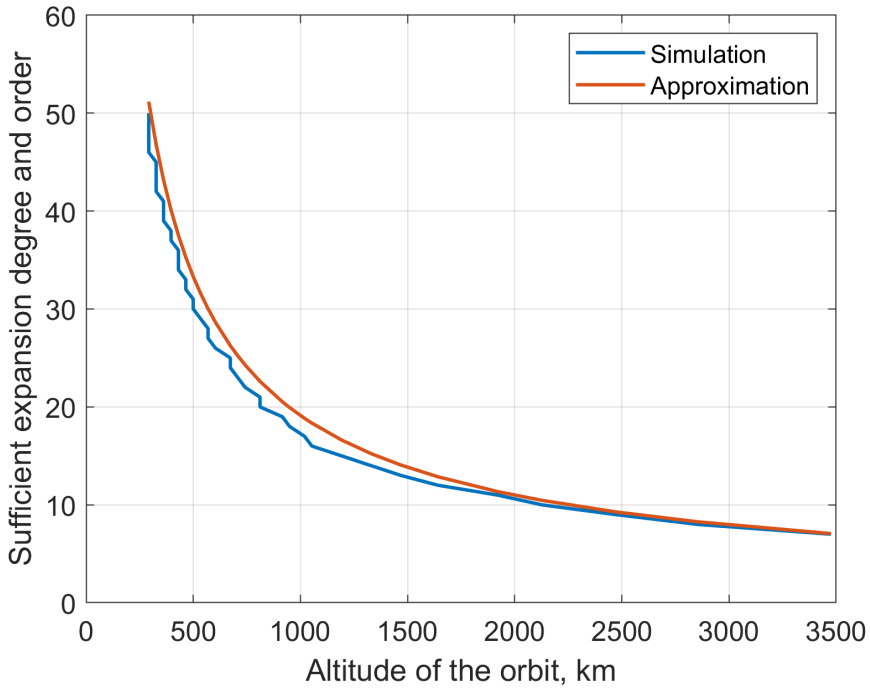

(b) $\varepsilon = 10^{-7}$

Fig. 2: Sufficient expansion degree and order of the lunar gravitational potential for different maximum relative magnitudes ε of the total perturbing acceleration.

III. LUNAR FROZEN ORBITS DESIGN

In this section, we describe the design of lunar frozen orbits, provide examples of frozen orbits, and select frozen orbits for the subsequent analyses.

Depending on the dynamical model considered, there exist several definitions of a frozen orbit. It seems reasonable to us to suggest the following unified definition: a frozen orbit is such an orbit that the eccentricity vector components $e_x = e\cos\omega$ and $e_y = \sin\omega$ are nearly constant. Fig. 3 shows some examples of lunar frozen orbits, plotted in polar coordinates (e, ω) for the inclination of 40°, altitude of 132 km, and different right ascensions of the ascending node (RAANs).

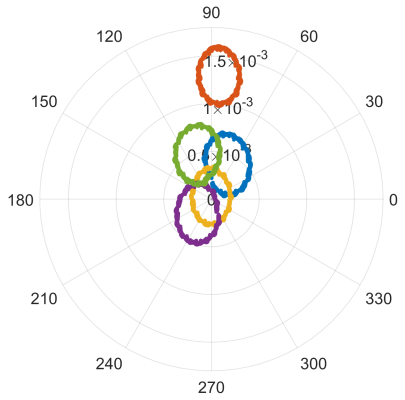

Fig. 3: One-year evolution of the eccentricity vector for 5 spacecraft in 132 km orbits whose planes are of 40° inclination and uniformly distributed in RAAN.

The problem of generating a frozen or quasi-frozen orbit is handled as an optimization problem which was inspired by [39]. Searching for a frozen orbit of given reference altitude h_{ref}, inclination i_0 and RAAN Ω_0 at the initial moment of time $t = 0$ is done by minimizing the objective function

$$J = (e_f - e_0)^2 + (\cos\omega_f - \cos\omega_0)^2 + (\sin\omega_f - \sin\omega_0)^2$$

over the semi-major axis a_0, eccentricity e_0, and argument of pericenter ω_0 values at the initial moment of time subject to constraints

$$a_0 \in [R + 0.9h_{\text{ref}}, R + 1.1h_{\text{ref}}],\ e_0 \in [0, e_{\max}],$$

where R km is the Moon radius, e_f and ω_f are the eccentricity and argument of pericenter at $t = t_f$ and $e_{\max}$ is such that $(R + 0.9h_{\text{ref}})(1 - e_{\max}) = R$. The first constraint means that only a slight variation in the semi-major axis is allowed to help the optimization algorithm to converge, while the second constraint relates to the minimum perilune distance. The orbital elements at $t = 0$ of $t = t_f$ are defined in the selenocentric orbital reference frame—the right-handed inertial frame with the x-axis along the Moon–Earth direction and z-axis along the orbital angular velocity of the Moon around the Earth at $t = 0$ or $t = t_f$, respectively.

In this research, $t_0 = 0$ corresponds to the midnight of Sep 1, 2021, $t_f = 365$ days, and the trajectory propagation is done by numerically integrating the equations of motion in the SCRS. The Bayesian optimization algorithm [49] (MATLAB's `bayesopt`) is used since it has demonstrated the highest performance in finding optimal solutions over both non-gradient and gradient methods.

The optimization procedure was set to stop when $J = \text{Tol} < 10^{-4}$ or the number of iterations exceeds 300. By setting the terminal tolerance Tol, we obtain the practically stable frozen orbits. For example, in Figs. 4 and 5, one can see a one-year evolution of the eccentricity vector for spacecraft in 15 uniform distributed orbital planes. All of them have a lifetime of at least several years, and, out of 15 orbits, six are frozen in a strict sense.

A set of (quasi-)frozen orbits have been calculated with different altitudes, inclinations, and RAANs. Specifically, we design medium-altitude frozen orbits $h_{\text{ref}} = 1392.3$ km which are in the 150:1 resonance with the lunar orbital motion and low-altitude frozen orbits ($h_{\text{ref}} = 131.5$ km, 325:1 resonance) with inclinations $i = 0°, 10°, 20°, \ldots, 90°$ and RAANs $\Omega = 0°, 12°, 24°, \ldots, 348°$. As a result, 2×271 one-year orbits have been obtained.

Since we study primarily low-altitude Walker–Mozhaev constellations, the standard Walker notation is adopted, with an additional letter for a low or medium altitude; for example, L80° : 180/15/1 means that a low-altitude constellation with totally 180 spacecraft in 15 planes with inclination 80° is considered. The last number $f = 1$ is the relative spacing between the satellites in adjacent planes: the change in true anomaly for equivalent satellites in neighbouring planes is equal to $f \times 360°/t$.

Now consider a constellation L[inc] : $n_s/n_p/1$. Let $\mathbf{x}_i(t)$ be phase state functions of the n_p frozen orbits with uniformly distributed RAANs and let P_i be the period of the i-th orbit (e.g., calculated at $t = t_0$). Then, for the sake of simplicity, we assume that the j-th spacecraft in the i-th plane has a phase state

$$\mathbf{x}_{ij}(t) = \mathbf{x}_i\left(t + P_i\left(\frac{j-1}{n_s/n_p} + \frac{i-1}{n_s}\right)\right),$$

where $i = 1, \ldots, n_p$ and $j = 1, \ldots, n_s/n_p$.

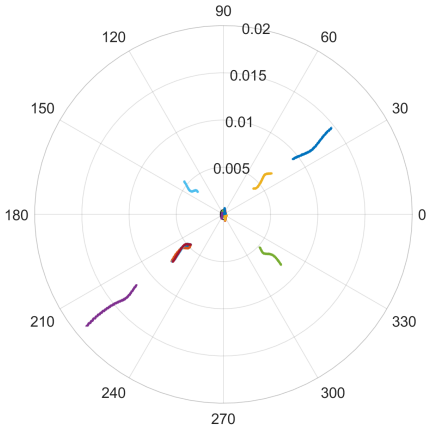

Fig. 4: One-year evolution of the eccentricity vector for 15 spacecraft in 132 km orbits whose planes are of 80° inclination and uniformly distributed in RAAN.

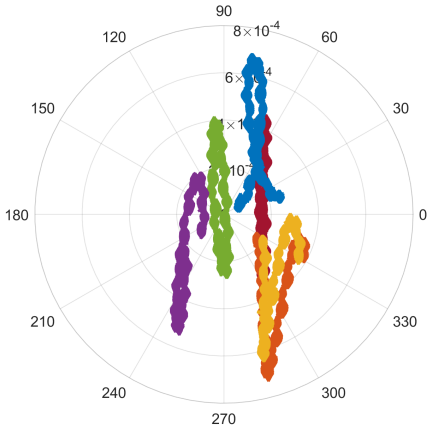

Fig. 5: One-year evolution of the eccentricity vector for the most stable (almost perfectly frozen) 6 orbits out of 15 orbits from the previous figure.

IV. COVERAGE ANALYSIS ROUTINES

In this section, we briefly describe the coverage geometry in terms of basic parameters (the antenna beam width, the footprint size, the elevation angle) and present a quasi-uniform surface grid generation technique for the global coverage analysis.

Let a spacecraft be at altitude h above the lunar surface. The antenna beam width α defines the footprint size φ and the minimum elevation angle β by the formulae (see Fig. 6)

$$\cos\beta = \frac{R+h}{R}\sin\frac{\alpha}{2},\quad \varphi = 90^\circ - \frac{\alpha}{2} - \beta.$$

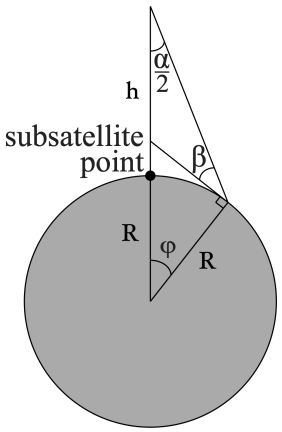

Fig. 6: Relation between the beam width, the footprint size, and the elevation angle.

For low lunar orbits (LLOs) considered in our research, we assume that the antenna beam width is sufficiently large. In this case, we set the minimum elevation angle to be 5°, i.e., $\beta \geq 5^\circ$. The footprint size can then be calculated as follows:

$$\varphi = 85^\circ - \sin^{-1}\left(\frac{R}{R+h}\cos 5^\circ\right).$$

Specifically, for the considered LLOs, $\alpha = 135.58^\circ$, $\beta = 5^\circ$, $\varphi = 17.21^\circ$.

For medium lunar orbits (MLOs), we assume the antenna beam width to provide the same level of antenna's radiation power as in a LLO. The antenna's radiation power is proportional to the solid angle Λ, that is proportional to $(h/R)^{-2}$. Hence, we get

$$\Lambda = 2\pi\left(1-\cos\frac{\alpha}{2}\right) \sim N \sim \frac{1}{(h/R)^2},$$

$$4\pi\sin^2\frac{\alpha}{4} \sim \frac{1}{(h/R)^2},$$

and, finally,

$$\frac{h}{R}\sin\frac{\alpha}{4} = \text{const}.$$

We calculated the constant (0.0424) for LLOs and used it to determine the antenna beam width for MLOs. As a result, we obtained $\alpha = 12.13^\circ$, $\beta = 79.03^\circ$, $\varphi = 4.91^\circ$.

To evaluate the global coverage, we use a quasi-uniform grid on a sphere which we generate by a numerical optimization procedure. Specifically, we search for vectors $\mathbf{r}_i \in \mathbb{R}^3$, $i = 1,\ldots,n$, that minimize the objective function

$$J = \sum_{1\leq i<j\leq n} \log\frac{1}{|\mathbf{r}_i - \mathbf{r}_j|}$$

subject to the constraints $|\mathbf{r}_i| = 1$, $i = 1,\ldots,n$ (inspired by [50]). For convenience of the subsequent

investigation, we fix the first six vectors $\mathbf{r}_1, \ldots, \mathbf{r}_6$ at positions $[\pm 1, 0, 0]^T$, $[0, \pm 1, 0]^T$, and $[0, 0, \pm 1]^T$, so it is possible to carry visibility analysis for the north and south poles and four points at the equator. Moreover, we fix $\mathbf{r}_7$ and $\mathbf{r}_8$ at positions of Boguslawsky (72.9°S 43.2°E) and Manzinus (67.7°S 26.8°E) craters. Technically, fixing is implemented by additional constraints in the optimization problem. For our analysis, we took $n = 1200$; the optimization problem was solved by the interior point method (MATLAB's `fmincon`). The result of the optimization is showed in Fig. 7. For each point in the grid and at every moment of time, one can determine if a spacecraft is visible from that point by taking into account the elevation angle and the altitude of the spacecraft orbit.

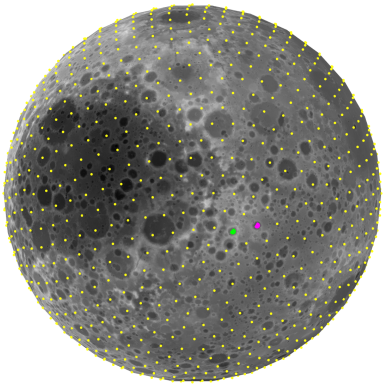

Fig. 7: Quasi-uniform surface grid of 1200 points which include the poles, the four equator points, and the Boguslawsky (green point) and Manzinus (purple point) craters.

V. COVERAGE ANALYSIS RESULTS

In this section, we provide the results of lunar surface coverage analysis for different constellations.

For a near-polar lunar orbit constellation, from geometry, we can estimate the theoretical minimum for the number of orbital planes and satellites in each plane to cover the lunar surface at every moment of time. For the low-lunar orbit constellation ($h_{\text{ref}} = 131.5$ km, $i = 80°$), the minimum number of orbital planes is

$$N_p = \left\lceil \frac{180°}{2\varphi} \right\rceil = 6$$

with minimum number of satellites in each plane

$$N_s = \left\lceil \frac{360°}{2\varphi} \right\rceil = 11,$$

where $\varphi = 17.21°$ is the footprint size estimated in the previous section. By numerical simulations, we computed the mean revisit time across the lunar surface, as it depends on the number of satellites in each plane and the number of planes (see Fig. 8). The results shown basically confirm the theoretical estimations.

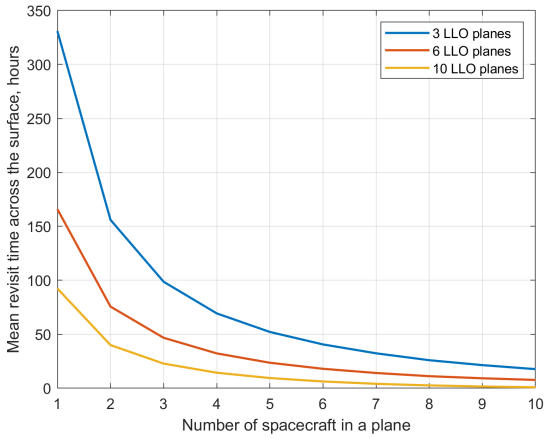

Fig. 8: Mean revisit time across the lunar surface as a function of the number of spacecraft in each plane and the number of planes.

The mean revisit time as function of the number of satellites was also obtained individually for the Boguslawsky and Manzinus craters (Figs. 9 and 10, respectively). Note that the mean revisit times obtained for the craters are several times less than the mean revisit times obtained across whole the lunar surface. In Figs. 11 and 12, the mean revisit times of the north and south poles are also presented.

The visibility properties at the north and south poles, as well as the craters, can be improved by adding spacecraft in a polar orbit. To avoid possible collisions with spacecraft in low altitude orbits, one can propose using a medium-altitude constellation of three satellites in one plane, i.e., M90° : 3/1/1. If the satellites in M90° : 3/1/1 have the same antenna's power as the ones in low altitude orbits, then the improvement in revisit times is insignificant. However, if the antenna's power allow a larger beam width so that the minimum elevation angle is 5°, then revisit times for the polar regions (including the specially considered craters) are significantly improved, as shown in Figs. 9, 10, 11, and 12.

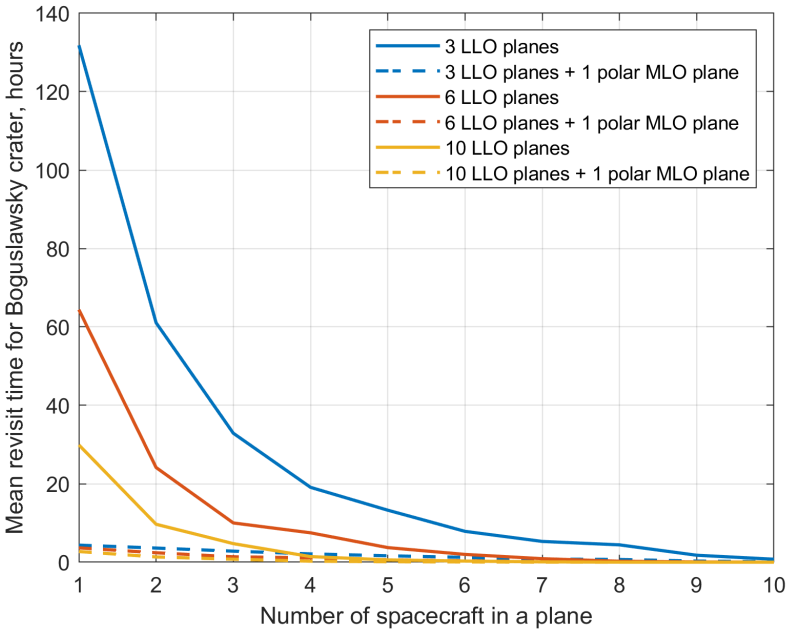

Fig. 9: Mean revisit time for Boguslawsky crater as a function of the number of spacecraft in each plane and the number of planes.

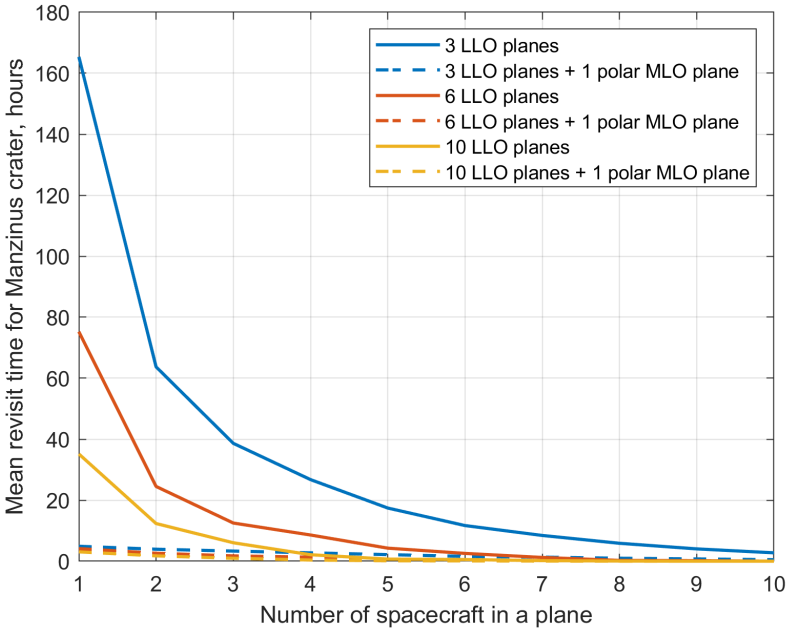

Fig. 10: Mean revisit time for Manzinus crater as a function of the number of spacecraft in each plane and the number of planes.

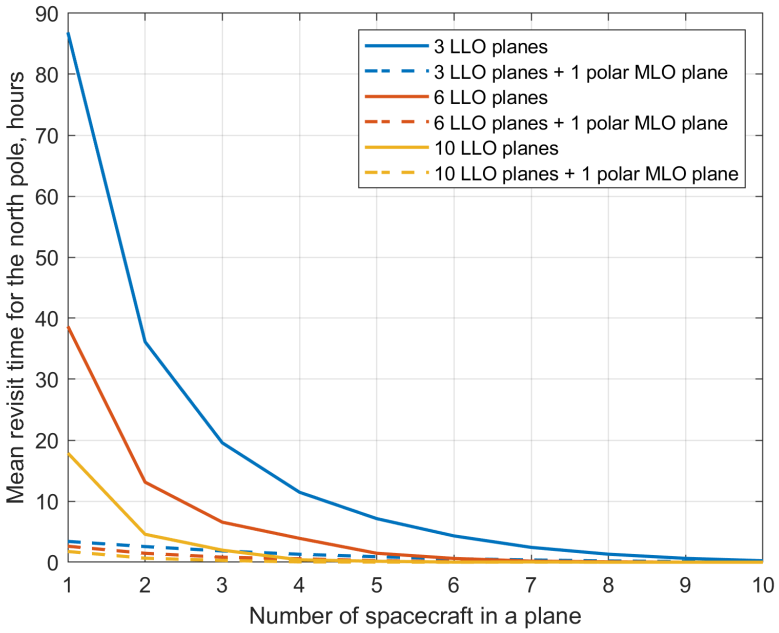

Fig. 11: Mean revisit time for the north pole as a function of the number of spacecraft in each plane and the number of planes.

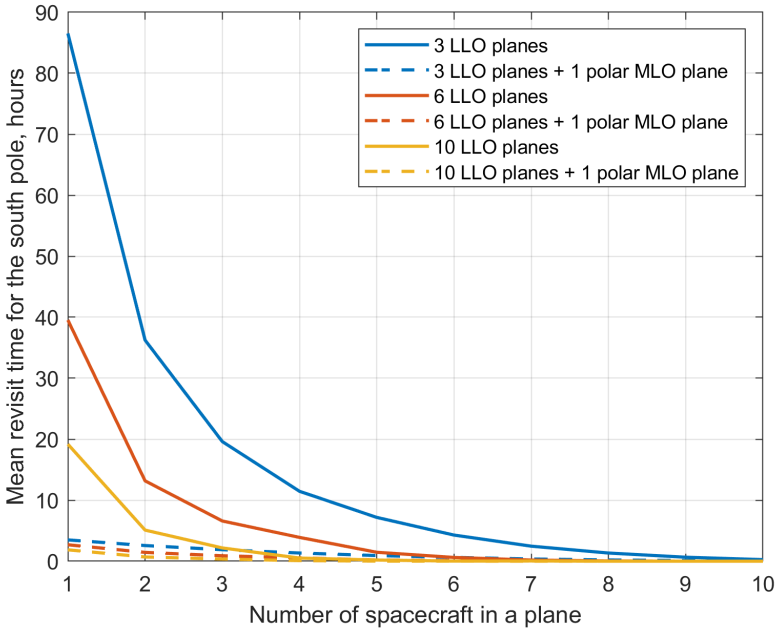

Fig. 12: Mean revisit time for the south pole as a function of the number of spacecraft in each plane and the number of planes.

Our investigations evidence that it is possible to provide the continuous 1-fold coverage of the lunar surface by the L80° : 180/15/1 constellation. In this case, the monthly averaged fraction of the surface visible at least by 2 spacecraft is 99.8%, while 3 and 4 satellites are visible from, respectively, 80.9% and 50.0% of the Moon. In Figs. 13 and 14, the fraction of the lunar surface visible at least by, respectively, 3 or 4 spacecraft is depicted as a function of time.

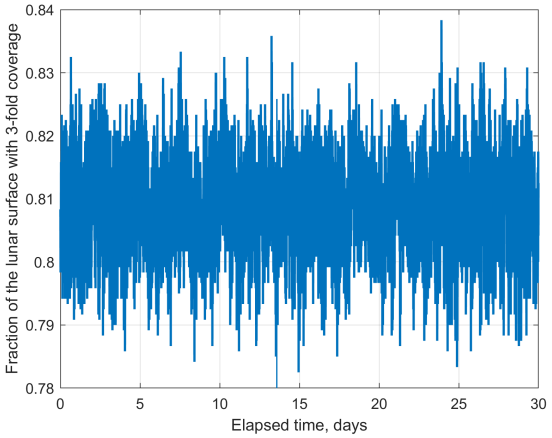

Fig. 13: Fraction of the lunar surface visible by at least 3 spacecraft for the L80° : 180/15/1 constellation. The mean value is 80.9%, the minimum is 78.0%, the maximum is 83.8%.

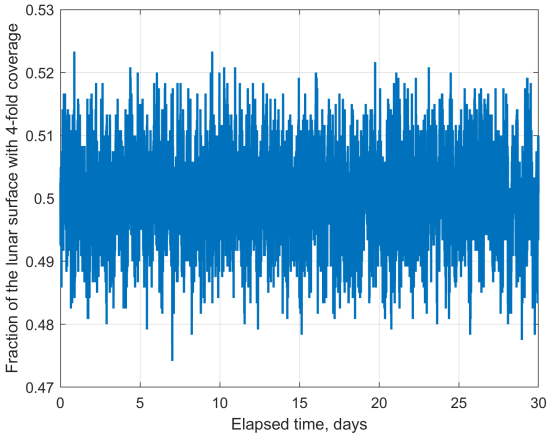

Fig. 14: Fraction of the lunar surface visible by at least 4 spacecraft for the L80° : 180/15/1 constellation. The mean value is 50.0%, the minimum is 47.4%, the maximum is 52.3%.

The analysis also shows that taking the L80° : 300/30/1 constellation instead of L80° : 180/15/1 provides the 4-fold continuous coverage of the lunar surface. However, for such a constellation, the minimum distance between the satellites equals 540 meters. The minimum distance in L80° : 180/15/1 equals 1.8 km and is considered affordable.

For each point in the surface grid, we also calculated the mean (over time) number of satellites visible from that point. The histogram for the mean number of visible satellites is depicted in Fig. 15. The analysis revealed that for the constellation L80° : 180/15/1, there exists around 1% of lunar surface for which at some times no satellites are visible. The constellation L80° : 300/15/1 provides the 2-fold coverage of the lunar surface (but not the 3-fold coverage). The constellation L80° : 375/15/1 provides the 3-fold coverage of the lunar surface and almost 97% of the lunar surface has at least the 4-fold coverage. The constellation L80° : 450/15/1 provides the 4-fold coverage of the lunar surface and 40% of the lunar surface has at least the 5-fold coverage.

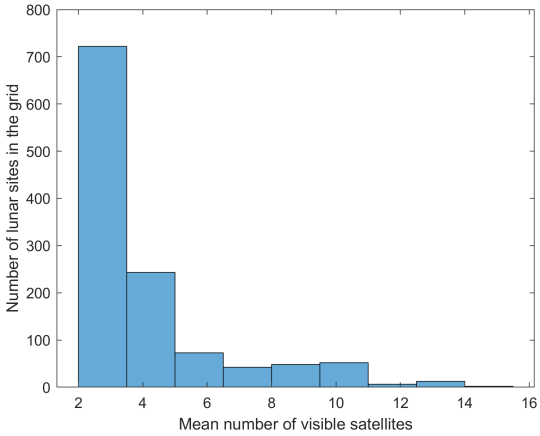

Fig. 15: Histogram for the mean (over time) number of visible satellites across the lunar surface (1200 grid points) for the L80° : 180/15/1 constellation.

In Figs. 16 and 17, we demonstrate the number of satellites visible from the Boguslawsky and Manzinus craters, respectively. The figures prove that the L80° : 180/15/1 constellation could provide continuous navigation at these craters and at least 6 spacecraft are visible anytime. The simulations also revealed that for continuous navigation at the craters, it is sufficient to use the L80° : 130/10/1 constellation.

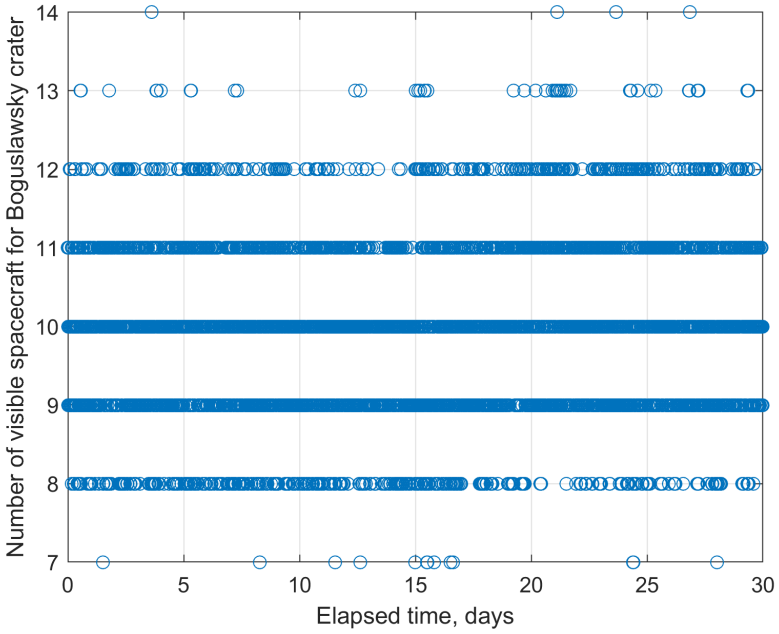

Fig. 16: Number of satellites visible at Boguslawsky crater for the L80° : 180/15/1 constellation.

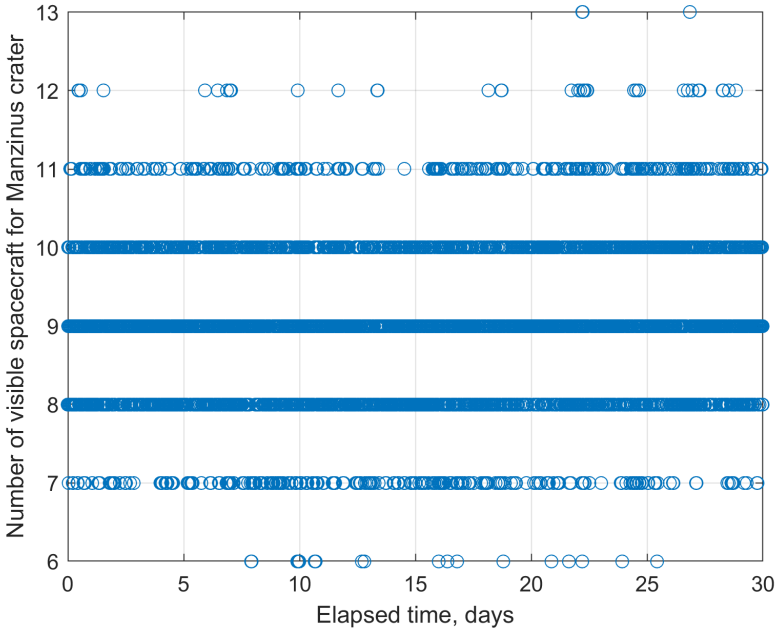

Fig. 17: Number of satellites visible at Manzinus crater for the L80° : 180/15/1 constellation.

VI. CONCLUSIONS

Using (quasi-)frozen low to medium lunar orbits is the only viable option for placing a lunar constellation of small satellites with no or limited resources for long-term station-keeping. In this study, we have put forward the practical approaches to solving the associated problems, from the choice of an accurate enough dynamical model to the generation of frozen and quasi-frozen (with a long enough lifetime) lunar orbits.

First, simple approximating formulas have been derived to relate the orbital altitude with the degree and order of the truncated expansion for the Moon's gravitational field required to adequately propagate such an orbit. Two threshold values for the relative magnitude of the ignored terms were considered; the power function approximation proved to be the best in both cases.

A robust numerical technique has been proposed to design long-lifetime low and medium lunar orbits. The differences in the eccentricity, $\cos\omega$, and $\sin\omega$ observed after a one-year propagation of the initial-guess orbit are squared and summed up to form the cost function. The Bayesian optimization algorithm (MATLAB's `bayesopt` function) shows the highest performance in this sort of extremely sensitive problems. Changing the terminal tolerance allowed us to obtain both perfectly frozen and quasi-frozen orbits. The latter are also important if one wants to achieve almost regular constellation geometry in a broadest range of inclinations and semimajor axes.

The coverage analysis for regular near-polar low-orbit constellations revealed that less than 100 small satellites equipped with low-gain omnidirectional or hemispherical antennas are capable to provide lunar communication services. For continuous navigation, it is required to deploy more than 300 satellites, but if the area to be covered is restricted to polar regions only, the total number of satellites can be reduced to as low as 130.

In case a higher power antenna is affordable for a small spacecraft, a low-altitude constellation can be effectively augmented with satellites in MLOs. Then the constellation size is substantially reduced (up to 100% for polar regions even with 3 additional satellites in a single polar MLO plane).

Many important problems relating to the use of small satellite constellations for communication and navigation purposes on the lunar surface have yet to be solved. Among them are the devising of efficient deployment schemes and the development of various end-of-life disposal scenarios. These problems are a subject of future studies.

VII. ACKNOWLEDGMENTS

This study is supported by the Russian Science Foundation (RSF) grant 19-11-00256.

REFERENCES

[1] Walker, J.G., "Some Circular Orbit Patterns Providing Continuous Whole Earth Coverage," Journal of the British Interplanetary Society, 1971, Vol. 24, pp. 369–384.

[2] Mozhaev, G.V. "The Problem of the Continuous Earth Coverage and the Kinematically Regular Satellite Networks, I," Kosmicheskie issledovaniya [Cosmic Research], 1972, Vol. 10, Issue 6, pp. 833–840.

[3] Mozhaev, G.V. "The Problem of the Continuous Earth Coverage and the Kinematically Regular Satellite Networks, II," Kosmicheskie issledovaniya [Cosmic Research], 1973, Vol. 11, Issue 1, pp. 59–69.

[4] Luders, R.D. "Satellite Networks for Continuous Zonal Coverage," American Rocket Society Journal, 1961, Vol. 31, pp. 179–184.

[5] Beste, D.C. "Design of Satellite Constellations for Optimal Continuous Coverage," IEEE Transactions on Aerospace and Electronic Systems, 1978, Vol. AES-14, Issue 3, pp. 466–473.

[6] Rider, L., "Analytic Design of Satellite Constellations for Zonal Earth Coverage Using Inclined Circular Orbits," The Journal of the Astronautical Sciences, 1986, Vol. 35, pp. 31–64.

[7] Lang T. J., Adams, W. S. "A Comparison of Satellite Constellations for Continuous Global Coverage," Mission Design and Implementation of Satellite Constellations, Space Technology Proceedings (Springer, Dordrecht), 1998, Vol. 1, pp. 62–70.

[8] Lansard, E., Frayssinhes, E., Palmade, J. "Global Design of Satellite Constellations: A Multi-Criteria Performance Comparison of Classical Walker Patterns and New Design Patterns," Acta Astronautica, 1998, Vol. 42, No. 9, pp. 555–564.

[9] Huang, S., Colombo, C., Bernelli-Zazzera, F. "Multi-Criteria Design of Continuous Global Coverage Walker and Street-of-Coverage Constellations Through Property Assessment," Acta Astronautica, 2021, Vol. 188, pp. 151–170.

[10] Ballard, A.H. “Rosette Constellations of Earth Satellites,” IEEE Transactions on Aerospace and Electronic Systems, 1980, Vol. AES-16, Issue 5, pp. 656–673.

[11] Draim, J. “Three- and Four- Satellite Continuous Coverage Constellations,” Journal of Guidance, Control, and Dynamics, 1985, Vol. 8, No. 6, pp. 725–730.

[12] Draim, J. “A Common Period Four-Satellite Continuous Coverage Constellation,” Journal of Guidance, Control, and Dynamics, 1987, Vol. 10, No. 5, pp. 492–499.

[13] Draim, J. “Continuous Global N-Tuple Coverage with (2N+2) Satellites,” Journal of Guidance, Control, and Dynamics, 1987, Vol. 14, No. 1, pp. 17–23.

[14] Ely, T., Crossley, W., Williams, E. “Satellite Constellation Design for Zonal Coverage Using Genetic Algorithms,” The Journal of the Astronautical Sciences, 1999, Vol. 47, No. 3–4, pp. 207–228.

[15] Ferringer, M.P., Spencer, D.B. “Satellite Constellation Design Tradeoffs Using Multiple-Objective Evolutionary Computation,” Journal of Spacecract and Rockets, 2006, Vol. 43, No. 6, pp. 1404–1411.

[16] Whittecar, W.R., Ferringer, M.P. “Global Coverage Constellation Design Exploration Using Evolutionary Algorithms,” AIAA/AAS Astrodynamics Specialist Conference, San Diego, CA , August 4–7, 2014, Paper AIAA 2014-4159, 20 p.

[17] Shtark, T., Gurfil, P. “Regional Positioning Using a Low Earth Orbit Satellite Constellation,” Celestial Mechanics and Dynamical Astronomy, 2018, Vol. 130, Article 14, 28 p.

[18] Ulybyshev, Y. “Satellite Constellation Design for Complex Coverage,” Journal of Spacecraft and Rockets, 2008, Vol. 45, No. 4, pp. 843–849.

[19] Ulybyshev, Y. “Geometric Analysis and Design Method for Discontinuous Coverage Satellite Constellations,” Journal of Guidance, Control, and Dynamics, 2014, Vol. 37, No. 2, pp. 549–557.

[20] Ulybyshev, Y. “General Analysis Method for Discontinuous Coverage Satellite Constellations,” Journal of Guidance, Control, and Dynamics, 2015, Vol. 38, No. 12, pp. 2475–2482.

[21] Razoumny, Y.N. “Fundamentals of the Route Theory for Satellite Constellation Design for Earth Discontinuous Coverage. Part 1: Analytic Emulation of the Earth Coverage,” Acta Astronautica, 2016, Vol. 128, pp. 722–740.

[22] Razoumny, Y.N. “Fundamentals of the Route Theory for Satellite Constellation Design for Earth Discontinuous Coverage. Part 2: Synthesis of Satellite Orbits and Constellations,” Acta Astronautica, 2016, Vol. 128, pp. 741–758.

[23] Razoumny, Y.N. “Fundamentals of the Route Theory for Satellite Constellation Design for Earth Discontinuous Coverage. Part 3: Low-Cost Earth Observation with Minimal Satellite Swath,” Acta Astronautica, 2016, Vol. 129, pp. 447–458.

[24] Razoumny, Y.N. “Route Satellite Constellations for Earth Discontinuous Coverage and Optimal Solution Peculiarities,” Journal of Spacecraft and Rockets, 2017, Vol. 54, No. 3, pp. 572–581.

[25] Razoumny, Y.N. “Fundamentals of the Route Theory for Satellite Constellation Design for Earth Discontinuous Coverage. Part 4: Compound Satellite Structures on Orbits with Synchronized Nodal Regression,” Acta Astronautica, 2016, Vol. 129, pp. 459–465.

[26] Mortari, D., Wilkins, M.P., Bruccoleri, C. “The Flower Constellations,” The Journal of the Astronautical Sciences, 2004, Vol. 52, pp. 107–127.

[27] Mortari, D., Wilkins, M.P. “The Flower Constellation Set Theory Part I: Compatibility and Phasing,” IEEE Transactions on Aerospace and Electronic Systems, 2008, Vol. 44, Issue 3, pp. 953–963.

[28] Wilkins, M.P., Mortari, D. “The Flower Constellation Set Theory Part II: Secondary Paths and Equivalency,” IEEE Transactions on Aerospace and Electronic Systems, 2008, Vol. 44, Issue 3, pp. 964–976.

[29] Avendaño, M.E., Davis, J.J., Mortari, D. “The 2-D Lattice Theory of Flower Constellations,” Celestial Mechanics and Dynamical Astronomy, 2013, Vol. 116, Issue 4, pp. 325–337.

[30] Davis, J.J., Avendaño, M.E., Mortari, D. “The 3-D Lattice Theory of Flower Constellations,” Celestial Mechanics and Dynamical Astronomy, 2013, Vol. 116, Issue 4, pp. 339–356.

[31] Arnas, D., Casanova, D., Tresaco, E. "4D Lattice Flower Constellations," Advances in Space Research, 2021, Vol. 67, Issue 11, pp. 3683–3695.

[32] Arnas, D., Casanova, D., Tresaco, E. "2D Necklace Flower Constellations," Acta Astronautica, 2018, Vol. 142, pp. 18–28.

[33] Arnas, D., Casanova, D., Tresaco, E. "2D Necklace Flower Constellations Applied to Earth Observation Missions," Acta Astronautica, 2021, Vol. 178, pp. 203–215.

[34] Arnas, D., Casanova, D., Tresaco, E., Mortari, D. "3-Dimensional Necklace Flower Constellations," Celestial Mechanics and Dynamical Astronomy, 2017, Vol. 129, Issue 4, pp. 433–448.

[35] Ely, T.A., Lieb, E. "Constellations of Elliptical Inclined Lunar Orbits Providing Polar and Global Coverage," AAS/AIAA Astrodynamics Specialist Conference, Lake Tahoe, CA, August 7-11, 2005, Paper AAS 05-343, 18 p.

[36] Ely, T.A. "Stable Constellations of Frozen Elliptical Inclined Lunar Orbits," The Journal of the Astronautical Sciences, 2005, Vol. 53, No. 3, pp. 301–316.

[37] Xu, M., Wang, J., Liu, S., Xu, S. "A New Constellation Configuration Scheme for Communicating Architecture in Cislunar Space," Mathematical Problems in Engineering, Volume 2013, Article ID 864950, 14 p.

[38] Gao, Z.-Y., Hou, X.-Y. "Coverage Analysis of Lunar Communication/Navigation Constellations Based on Halo Orbits and Distant Retrograde Orbits," The Journal of Navigation, 2020, Vol. 73, Issue 4, pp. 932–952.

[39] Folta, D., Quinn, D. "Lunar Frozen Orbits," AIAA/AAS Astrodynamics Specialist Conference and Exhibit, Keystone, CO, August 21-24, 2006, Paper AIAA 2006-6749, 18 p.

[40] Gordienko, E.S., Ivashkin, V.V., Simonov, A.V. "Analysis of Stability of Orbits of Artificial Lunar Satellites and Configuring of a Lunar Satellite Navigation System," Solar System Research, 2017, Vol. 51, No. 7, pp. 654–668.

[41] Thompson, J.R., Haygood, H.G., Kezirian, M.T. "Design and Analysis of Lunar Communication and Navigation Satellite Constellation Architectures," AIAA SPACE 2010 Conference & Exposition, Anaheim, CA, August 30 – September 2, 2010, Paper AIAA 2010-8644, 14 p.

[42] Oleson, S.R., McGuire, M.L. "COMPASS Final Report: Lunar Network Satellite-High Rate (LNS-HR)," NASA Technical Memorandum TM—2012-217139, 2012, 114 p.

[43] Mikrin, E.A., Mikhailov, M.V., Orlovskii, I.V., Rozhkov, S.N., Krasnopol'skii, I.A. "Satellite Navigation of Lunar Orbiting Spacecraft and Objects on the Lunar Surface," Gyroscopy and Navigation, 2019, Vol. 10, No. 2, pp. 54–61.

[44] McManus, L., Schaub, H. "Establishing a Formation of Small Satellites in a Lunar Flower Constellation," The Journal of the Astronautical Sciences, 2016, Vol. 63, pp. 263–286.

[45] Elipe, A., Lara, M. "Frozen Orbits About the Moon," Journal of Guidance, Control, and Dynamics, 2003, Vol. 26, No. 2, pp. 238–243.

[46] Lara, M., Ferrer, S., De Saedeleer, B. "Lunar Analytical Theory for Polar Orbits in a 50-Degree Zonal Model Plus Third-Body Effect," The Journal of the Astronautical Sciences, 2009, Vol. 57, No. 3, pp. 561–577.

[47] Lara, M. "Design of Long-Lifetime Lunar Orbits: A Hybrid Approach," Acta Astronautica, 2011, Vol. 69, Issues 3-4, pp. 186–199.

[48] Nie, T., Gurfil, P. "Lunar Frozen Orbits Revisited," 2018, Vol. 130, Article 61, 35 p.

[49] Snoek, J., Larochelle, H., Adams, R.P. "Practical Bayesian Optimization of Machine Learning Algorithms." arXiv:1206.2944, 2012.

[50] Lee, S., Mortari, D. "Quasi-equal area subdivision algorithm for uniform points on a sphere with application to any geographical data distribution," Computers and Geosciences, 2017, Vol. 103, pp. 142–151.